ACI STRUCTURAL JOURNAL TECHNICAL PAPER

Title No. 121-S42

Cyclic Behavior of Beams with Double-Perimeter and Continuous-Stirrup Hoops

by Yu-Chen Ou, Hermawan Sutejo, Jyun-Lin Huang, and Sheng-I Yen

Two types of hoop layouts, double-perimeter hoops (DPH) and continuous-stirrup hoops (CSH), were examined in this research for beams of special moment frames. Compared to conventional hoops (CH), the DPH and CSH have the advantage of better constructability. Full-scale beam specimens—specimen CH as a control specimen and specimens DPH and CSH as test specimens—were tested using lateral cyclic loading to examine their seismic performance. Test results showed that although specimen DPH violated the Code requirement for the number and spacing of laterally supported longitudinal bars, the specimen still exhibited seismic performance sufficient for beams of special moment frames. Specimen CSH showed better seismic performance than the control specimen (CH). The better performance of CSH was mainly attributed to the better concrete confinement and reinforcing bar buckling restraint ability of the intermediate hoops of the CSH than the intermediate stirrups of the CH.

Keywords: closed stirrups; deformation capacity; energy dissipation; hoops; plastic hinge region; reinforced concrete beams; reinforcement buckling; special moment frames.

INTRODUCTION

It is stated in ACI 318-19[1] that in the potential plastic hinge region of beams of special moment frames, transverse reinforcement should be provided in the form of hoops. The spacing of the hoops should not exceed $d/4$, 150 mm (6 in.), and $6d_b$ for Grade 420 MPa (60 ksi) longitudinal bars. Moreover, every corner and alternate longitudinal bar closest to the tension and compression faces should be laterally supported by transverse reinforcement. In addition, the spacing of the laterally supported longitudinal bars (h_x) should not be more than 350 mm (14 in.). These requirements are intended to provide good concrete confinement to increase concrete strength and deformation capacities and to provide sufficient lateral support for longitudinal bars to prevent premature buckling in compression.

To improve the constructability, the hoop is allowed to be formed by a U-stirrup having seismic hooks at both ends and closed by a crosstie. A typical transverse reinforcement layout used in Taiwan that satisfies the aforementioned requirements is shown in Fig. 1(a). This layout is referred to as conventional hoops (CH) herein and consists of a perimeter stirrup and an intermediate stirrup. Both stirrups have seismic hooks at the ends. The two stirrups are closed by a crosstie on the top. The construction proceeds in the following steps (Fig. 2): a) placing the two top-corner longitudinal bars and then installing the perimeter stirrups with the hooks of the stirrups hanging on the two top longitudinal bars; b) placing the two bottom-corner longitudinal bars; c) placing the two intermediate top longitudinal bars and then installing the intermediate stirrups hanging on the two longitudinal bars; d) placing the rest of the bottom longitudinal bars; e) placing the rest of the top longitudinal bars; and f) placing the crossties to close the stirrups. All reinforcing bars were secured together in place by tie wire. Note that the aforementioned construction is conducted on site after the floor and beam formwork is set. Thus, the space for beam reinforcement work is limited as reinforcing bars can only be placed from the top side of the beam. The intermediate stirrups further increase the difficulty of bar placement and limit the space for bar tying. As a result, many construction companies in Taiwan are reluctant to construct intermediate stirrups. If the shear design requires four legs of stirrups, two pieces of perimeter stirrups would be used instead of intermediate stirrups, as shown in Fig. 1(b). This type of transverse reinforcement is referred to as double-perimeter hoops (DPH) herein. The construction of DPH proceeds in the following steps (Fig. 3): a) placing the two top-corner longitudinal bars and then installing the perimeter stirrups (two in a set) with the hooks of the stirrups hanging on the two top longitudinal bars; b) placing all the bottom longitudinal bars; c) placing the rest of the top longitudinal bars; and d) placing the crossties to close the stirrups. Because there is no interference from the intermediate stirrups, the space for the placement and tying of reinforcing bars is maximized, and construction time is reduced. The DPH can satisfy the requirements for shear and the maximum spacing between hoops. However, they often fail to satisfy the requirements that every alternate longitudinal bar should be laterally supported, and often violate the maximum h_x requirement (350 mm [14 in.]).

The requirement that every alternate longitudinal bar needs to be laterally supported is mainly intended to reduce the buckling tendency of longitudinal bars in compression. The maximum h_x requirement is primarily to ensure confinement effectiveness by limiting the span of confined concrete arches.[2] These requirements were originally developed for columns[3,4] and first appeared in ACI 318-63.[5] These requirements were extended to the plastic hinge region of beams of special moment frames in ACI 318-83.[6] In ACI 318-14, the requirements were made stricter by requiring lateral support

ACI Structural Journal, V. 121, No. 3, May 2024.
MS No. S-2023-105.R1, doi: 10.14359/51740485, received November 26, 2023, and reviewed under Institute publication policies.

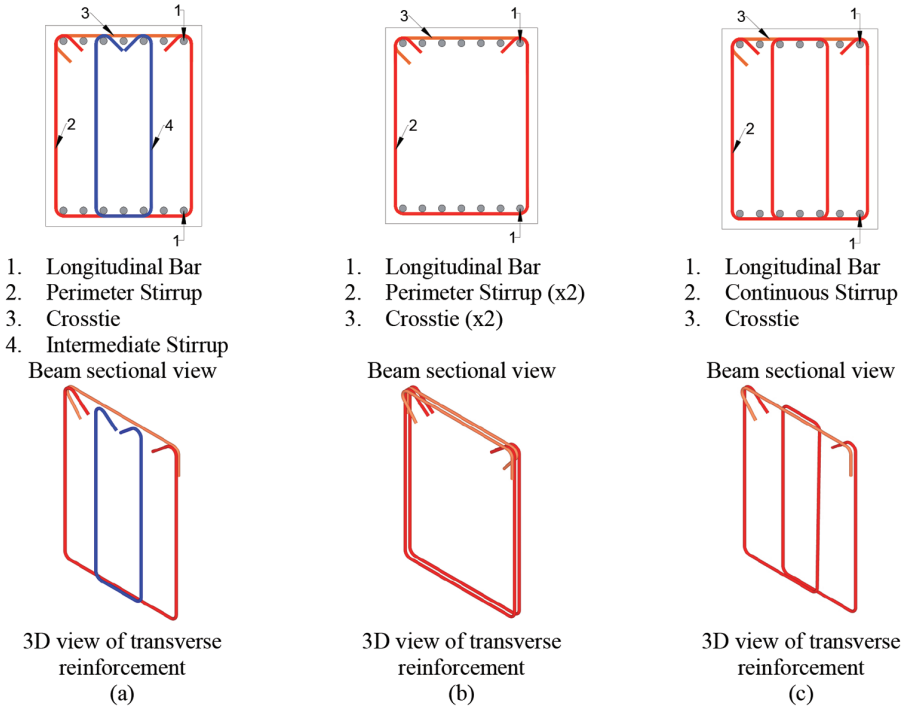

Fig. 1—Transverse reinforcement layouts: (a) CH; (b) DPH; and (c) CSH.

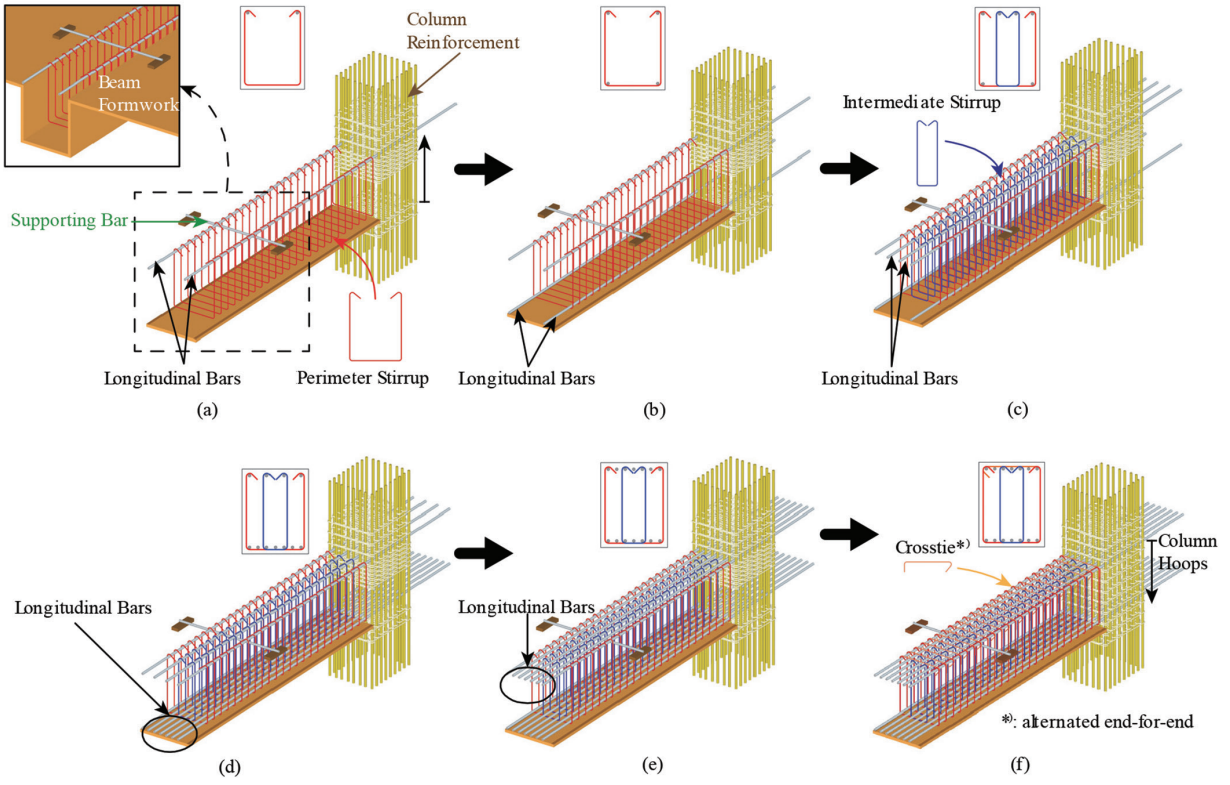

Fig. 2—Construction procedure for CH.

for every longitudinal bar and limiting h_x to 200 mm (8 in.) for the plastic hinge region of the columns of special moment frames when $P_u > 0.3A_g f_c'$ or $P_u > 70$ MPa (10,000 psi). This change is mainly based on the research by Elwood et al.[7,8]

Compared with the abundant test data on columns, no tests to the authors' knowledge were conducted to examine the effect of the number and spacing of laterally supported longitudinal bars on the seismic behavior of beams. Visnjic et al.[9] examined the effect of hoop spacing on the seismic performance of large beams. As a result of this research, one of the upper limits of the hoop spacing, 305 mm (12 in.), was reduced to 152 mm (6 in.) in ACI 318-11[10] to delay the buckling of longitudinal bars of large beams. Note that in Visnjic et al.'s study, the number and spacing of laterally supported longitudinal bars satisfy the Code requirements. Beams are typically subjected to a negligible or small axial

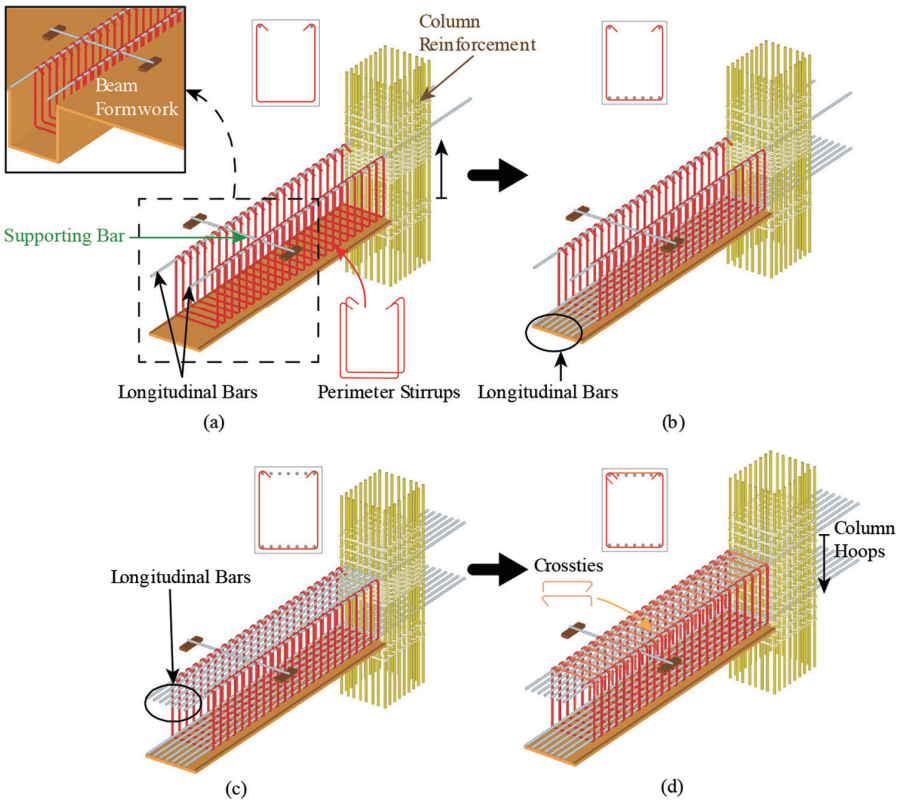

Fig. 3—Construction procedure for DPH.

compressive load of less than $0.1A_g f_c'$. Some engineers argue that the Code requirements for the number and spacing of laterally supported longitudinal bars in the potential plastic hinge region may be relaxed, provided that the spacing of hoops satisfies the Code requirement. Therefore, the first objective of this research was to examine this possibility by comparing the seismic performance of a beam with the CH (Fig. 1(a)) and the DPH (Fig. 1(b)). The second objective of this research was to examine the seismic performance of a beam with the proposed continuous-stirrup hoops (CSH), as shown in Fig. 1(c). The proposed hoops improve the constructability of the transverse reinforcement and satisfy the Code requirement for the number and spacing of laterally supported longitudinal bars.

Continuous-stirrup hoops

As shown in Fig. 1(c), each set of CSH consists of a single-bar continuous stirrup with seismic hooks at both ends and a crosstie to close the continuous stirrup. The continuous stirrup runs continuously to form a perimeter stirrup and an intermediate hoop. The construction of the hoops proceeds in the following steps (Fig. 4): a) placing the two top-corner longitudinal bars and then placing all the continuous stirrups near the column side with the hooks of the stirrups hanging on the two longitudinal bars; b) placing the bottom and then the top longitudinal bars within the intermediate hoops of the continuous stirrups; c) moving the continuous stirrups one by one to their design locations; d) placing the rest of the bottom and top longitudinal bars; and e) placing the crossties to close the stirrups. Compared to the CH (Fig. 1(a)), the CSH have the advantage of reducing installation time as the intermediate hoop is installed together with the perimeter stirrup.

The use of beam continuous-hoop reinforcement, in which the transverse reinforcement of the entire beam is formed by one continuously wound bar, to increase the constructability of beam transverse reinforcement has been examined in several previous studies.[11-16] Tests conducted using monotonic and cyclic loading have shown beams with continuous-hoop reinforcement can have better structural performance than beams with conventional transverse reinforcement.[15] However, such continuous-hoop reinforcement does not have the intermediate hoop required in this research.

RESEARCH SIGNIFICANCE

The intermediate stirrups of CH in beams of special moment frames often cause construction difficulty. Two types of hoop layouts (DPH and CSH) with better constructability than the CH were proposed in this research to address the issue. Results of tests using full-scale specimens showed that beams with the proposed hoop layouts could develop sufficient seismic performance for use in special moment frames.

EXPERIMENTAL PROGRAM

Specimen design

Three full-scale beam specimens were tested in this research. The beams were designed based on applicable provisions of beams of special moment frames of ACI 318-19.[1] The dimensions and reinforcement details of the specimens are shown in Fig. 5. The material properties of the specimens are listed in Table 1. Specimen CH had the conventional hoops (CH), as shown in Fig. 1(a), as transverse reinforcement and served

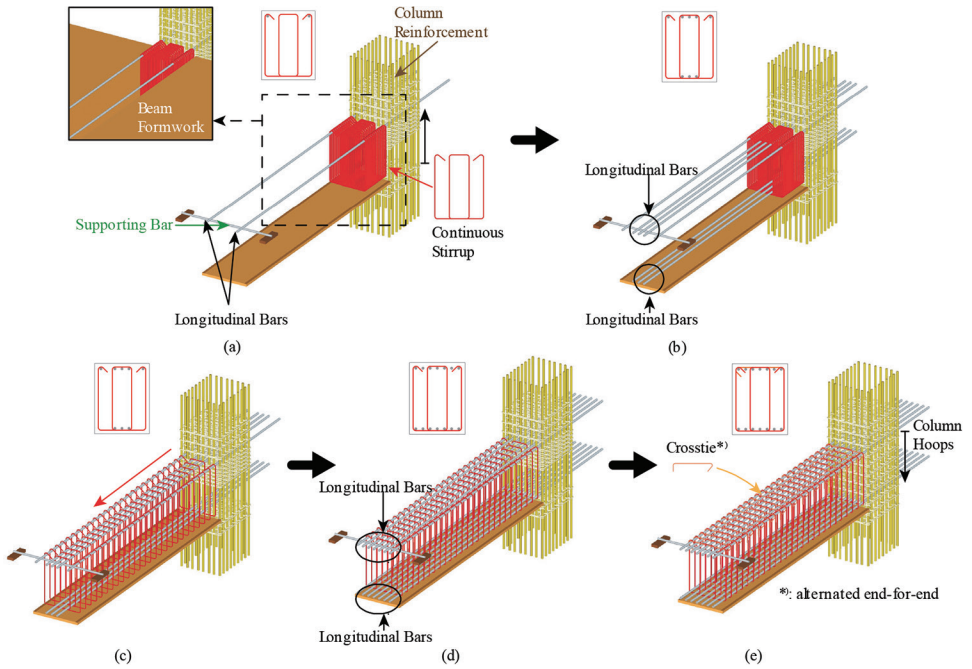

Fig. 4—Construction procedure for CSH.

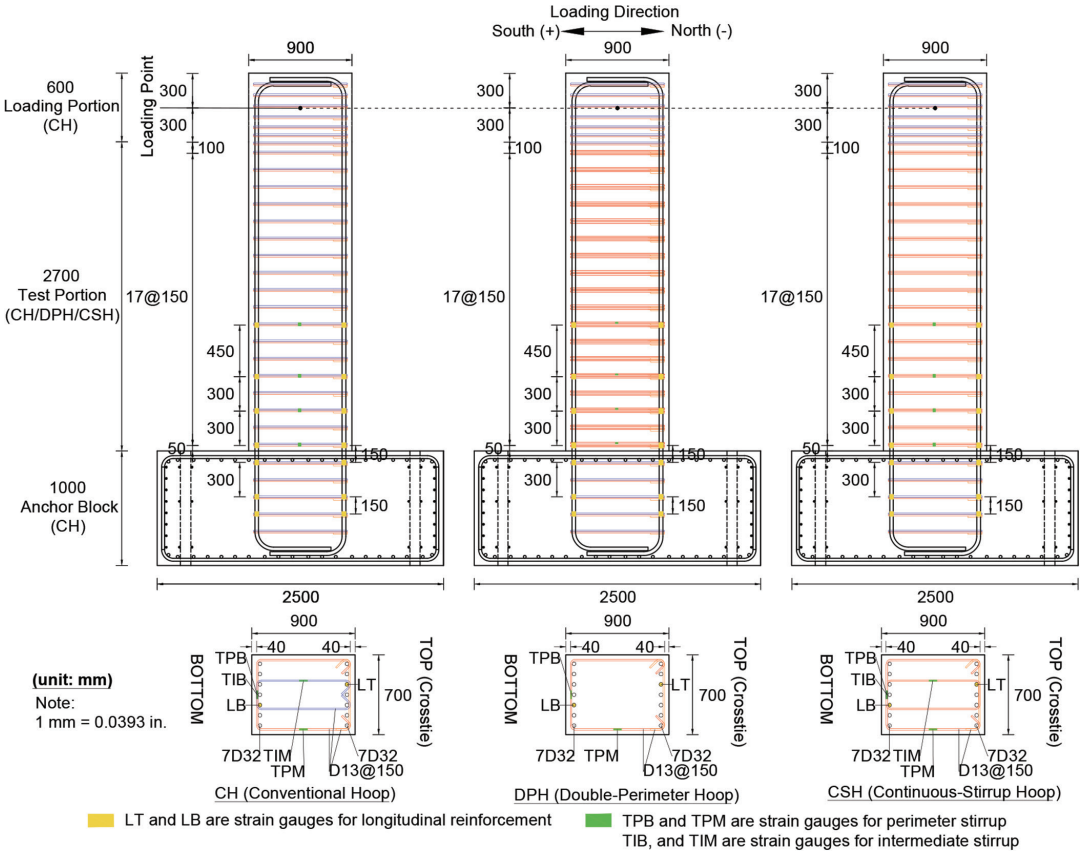

Fig. 5—Specimen design.

as a control specimen. Specimen DPH was designed with the double-perimeter hoops (DPH), as shown in Fig. 1(b), as transverse reinforcement, and specimen CSH had the continuous-stirrup hoops (CSH), as shown in Fig. 1(c), as transverse reinforcement. Figures 6(a) to (c) show the photos of the top side view of the reinforcing bar cages, and Fig. 6(d) to (f) show the top-corner view of the reinforcing bar cages. For specimen DPH, the central five top and bottom longitudinal bars did not have lateral support from the seismic hooks of transverse reinforcement, which violated the Code requirement that every alternate longitudinal bar should be laterally supported. Moreover, the h_x of the DPH was 562 mm (22.13 in.), which violated the maximum h_x requirement (350 mm [14 in.]). Comparing the seismic behavior of specimens

Table 1—Material properties

Specimen	Concrete		Longitudinal reinforcement				Perimeter hoop			Intermediate stirrup or hoop		
	f_{cs}', MPa	f_c', MPa	f_{yls}, MPa	f_{yl}, MPa	f_{ul}, MPa	ρ_l, %	f_{yps}, MPa	f_{yp}, MPa	f_{up}, MPa	f_{yis}, MPa	f_{yi}, MPa	f_{ui}, MPa
CH	35	51.7	420	462	669	0.98 (7D32)	420	474	666	420	474	666
DPH		49.5								—		
CSH		48.7								420	474	666

Note: 1 MPa = 0.145 ksi.

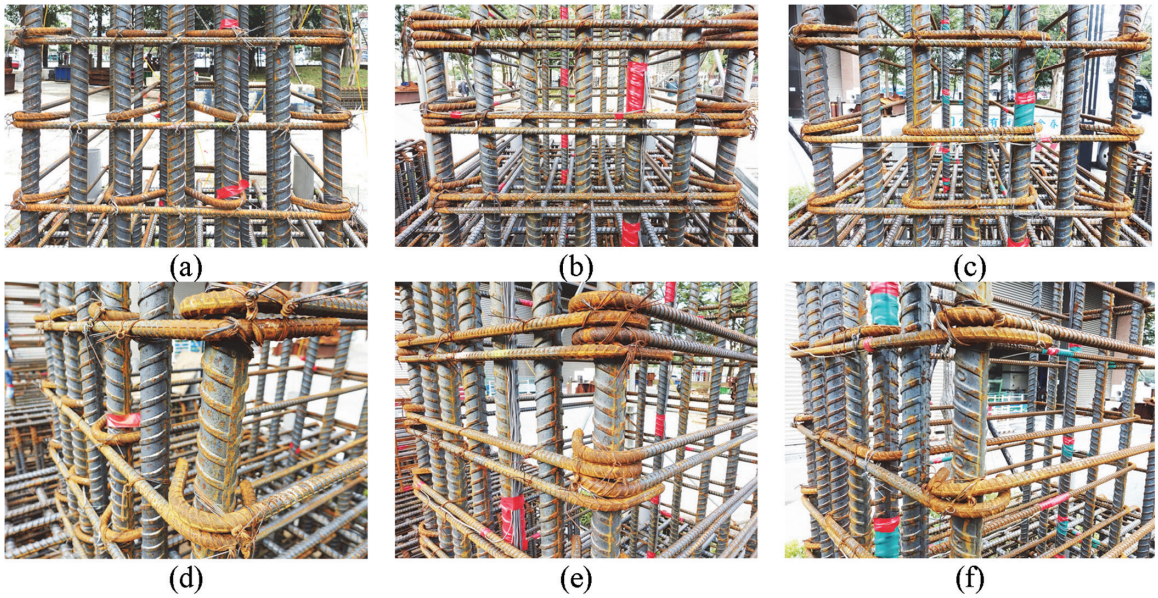

Fig. 6—Photos of reinforcing bar cages: top side view of specimens (a) CH, (b) DPH, and (c) CSH; and top-corner side view of specimens (d) CH, (e) DPH, and (f) CSH.

DPH and CH would reveal the effect of violating the aforementioned Code requirements on the seismic performance of the beam. Furthermore, comparing the seismic behavior of specimens CSH and CH would reveal the seismic performance of the CSH.

All the specimens had the same beam cross-sectional dimensions of 700 x 900 mm (27.6 x 35.4 in.) (width x height). The thickness of the concrete cover was 40 mm (1.57 in). Normalweight concrete with a specified compressive strength (f_{cs}') of 35 MPa (5.076 ksi) was used for all the specimens. SD 420W steel deformed bars, which have a material specification similar to ASTM A706 Grade 60 deformed bars,[17] were used for all longitudinal and transverse reinforcing bars. These cross-sectional dimensions and material strengths are typical for beams at the lower stories of 15-story buildings with a span length of approximately 8 to 9 m (26.2 to 29.5 ft) in the Taipei region of Taiwan.

For all the specimens, the distance from the loading point to the beam fixed end was 3000 mm (118.11 in.). The resulting shear span-effective depth ratio (a/d) was 3.6, falling into the category of slender beams. The beam was designed with seven D32 (a diameter of 32 mm [1.27 in.]) longitudinal bars on the top and bottom sides of the cross section. The top and bottom sides of the cross section are also referred to as the north and south sides (refer to Fig. 5), respectively. The seven D32 bars resulted in a longitudinal tension reinforcement ratio (ρ_l) of 0.98%. The transverse reinforcement of the beam was designed so that the shear demand (V_u) calculated based on $1.25f_{yls}$ was close to the design shear strength (ϕV_n) to critically evaluate the seismic performance of the beams. Moreover, the spacing of hoops needs to satisfy the maximum spacing requirement ($d/4$, 150 mm [6 in.], and $6d_b$) for the potential plastic hinge region. Considering these requirements and using D13 (a diameter of 13 mm [0.5 in.]) reinforcing bars, the spacing of the transverse reinforcement was determined to be 150 mm (5.91 in.). This resulted in a shear demand-capacity ratio ($V_u/\phi V_n$) of 0.85 to 0.87.

Test setup and instrumentation

The specimens were tested in an upright, cantilever fashion, as shown in Fig. 7. The end block of the specimen was fixed to the strong floor by post-tensioning. Lateral cyclic loading satisfying ACI 374.1-05[18] was applied to the free end of the specimen beam. The loading was displacement-controlled to drift levels of 0.25, 0.375, 0.5, 0.75, 1.0, 1.5, 2.0, 3.0, 4.0, 5.0, 6.0, 7.0, and 8.0%. Positive loading was defined as laterally pulling the beam so that the top side of the beam (north side) was in tension and the bottom side (south side) was in compression. Each drift level was repeated in three cycles to observe the degradation of strength and stiffness in each drift level. The test was conducted until the load dropped to less than 50% of the peak load.

Strain gauges were installed on the transverse and longitudinal reinforcement, as shown in Fig. 5, to measure the

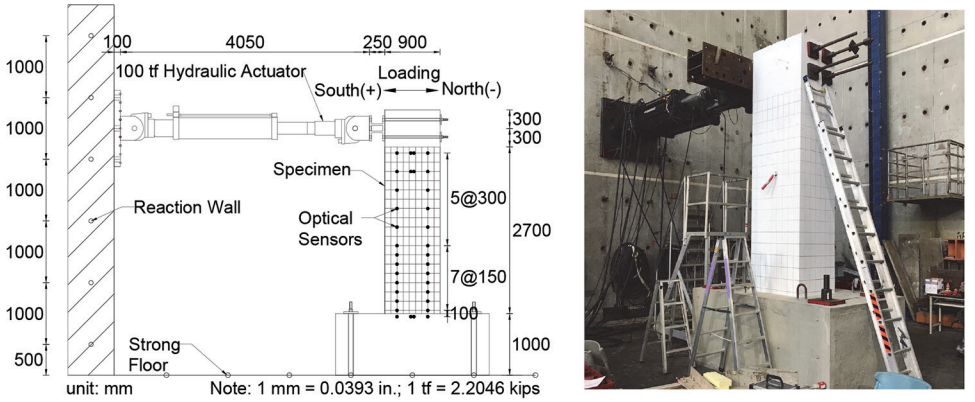

Fig. 7—(a) Test setup; and (b) photo of test setup.

induced strain in the reinforcement. Optical sensors were attached to the east face of the specimen. These sensors allowed an optical receiver to track their space coordinates during testing. These coordinate data were used to calculate the deformations of the beam, including curvature and shear strains.

TEST RESULTS AND DISCUSSION

Damage process

For all three specimens, flexural cracks first appeared at 0.25% drift. At 0.375% drift, some flexural cracks started to turn inclined to become flexural-shear cracks. The extent, number, and width of the cracks increased with increasing drift levels. At the end of the first cycle of 3% drift loading, extensive flexural and flexural-shear cracks were observed for all three specimens. No significant differences in behavior were found between the three specimens.

After the first cycle of the 4% drift loading, significant differences in behavior appeared between the three specimens. The differences mainly occurred around the top side of the beam (north side). Note that crossties were used on this side. The differences can be observed from the east side view of the specimen (the side face of the beam), as shown in Fig. 8(a) to (c), and the north side view of the specimen (the top face of the beam), as shown in Fig. 8(d) to (f), for specimens CH, DPH, and CSH, respectively. Specimen CH showed clear bulging on the north face, likely due to the pushing from the concrete expansion and buckling of longitudinal bars in compression. Specimen DPH exhibited extensive concrete spalling, exposing buckled longitudinal bars and loosened crossties (popping out from the 90-degree end). Specimen CSH showed damage less severe than the other two beams. No significant bulging nor spalling of concrete was observed. The damage condition of specimen CSH demonstrated that the intermediate hoops of specimen CSH were more effective in confining concrete and restraining the buckling of longitudinal bars than the conventional intermediate stirrups of specimen CH. The intermediate hoops of specimen CSH are formed by one continuous bar and hence can provide better restraint to longitudinal bars within the hoop than the conventional intermediate stirrups. Specimen DPH showed the most severe damage. This was true despite two crossties being used for each set of DPH. In contrast, one crosstie was used for each set of CH and CSH. It appeared that the crossties alone could not effectively restrain the buckling of the central five longitudinal bars at 4% drift. As a result, specimen DPH showed a significant drop in the lateral load at the peak negative 4% drift when the top side of the beam was in compression. Hence, in the negative drift loading, specimen DPH reached the peak applied load at 3% drift, earlier than the other two specimens.

The damage around the bottom side (south side) of the beam was generally less than that around the top side for all three specimens. This was because crossties were not used for the bottom sides, and the lateral support of all the supported bottom longitudinal bars was provided by the corners of hoops or stirrups rather than seismic hooks. The three specimens did not show significant differences in damage around the bottom side of the beam, although specimen DPH did show slightly more severe bulging than the other two specimens (Fig. 8(b)). The lateral load was still increasing for all three specimens in the positive loading direction when the bottom side of the beam was in compression.

After the first cycle of 5% drift, severe damage involving concrete spalling, longitudinal bar buckling, and loosening of crossties and stirrup hooks could be observed around the top side of the beam (north side) for all three specimens, as shown in Fig. 9. At this drift and in the negative loading direction when the top side of the beam was in compression, specimens CH and CSH showed a significant drop in the lateral load. Therefore, in the negative loading direction, both specimens reached their peak lateral load at 4% drift. A comparison of the damage conditions showed that specimen DPH showed the worst buckling behavior. The top five central longitudinal bars buckled almost uniformly outward (Fig. 9(h)). These bars were only restrained from buckling by crossties, which tended to pop out from the 90-degree end once the cover concrete spalled. Only the two top-corner longitudinal bars were better restrained by the seismic hooks of the perimeter stirrups. For specimen CSH, the top five longitudinal bars, including the two top-corner bars and the three bars within the intermediate hoops, were effectively restrained to resist buckling (Fig. 9(i)). In contrast, for specimen CH, four top longitudinal bars, including the two top-corner bars and the two bars laterally supported by the seismic hooks of the intermediate stirrups, were effectively

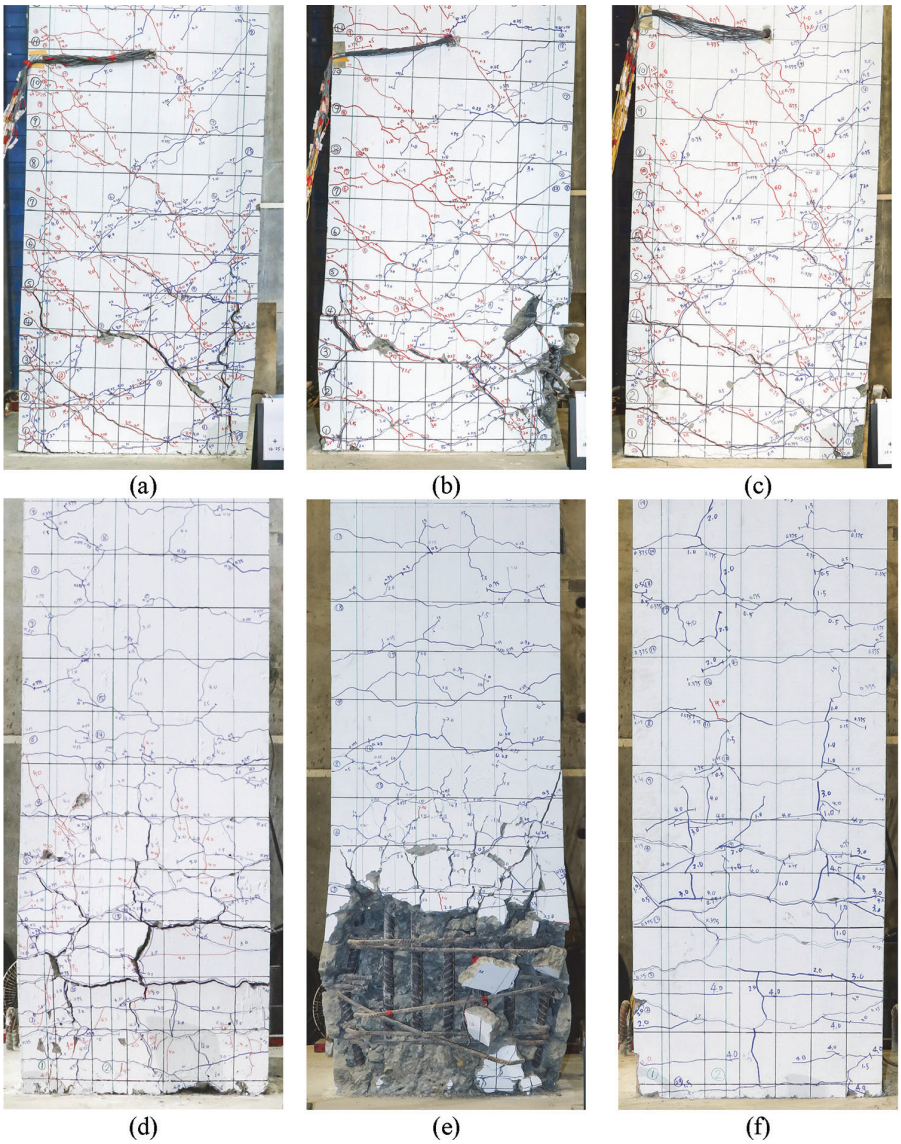

Fig. 8—Damage condition after first cycle of 4% drift on east face (side face) of beam near fixed end for specimens (a) CH, (b) DPH, and (c) CSH; and on north face (top face) of beam for specimens (d) CH, (e) DPH, and (f) CSH.

restrained from buckling (Fig. 9(g)). Therefore, specimen CSH, with one more longitudinal bar effectively restrained than specimen CH and better restraint ability of intermediate hoops than the intermediate stirrups of specimen CH, showed a smaller extent of concrete damage and less severity of buckling of longitudinal bars than specimen CH.

The damage around the bottom side of the beam was again less severe than that around the top side for all three specimens (Fig. 9(a) to (c)) after the first cycle of 5% drift. Specimen DPH showed severe concrete spalling around the bottom side. The lateral load in the positive loading direction dropped significantly at 5% drift compared to the previous drift. Hence, the peak lateral load in the positive loading direction of specimen DPH occurred at 4% drift. The damage condition of specimen CH around the bottom side was better than that of specimen DPH. Only some bulging of cover concrete was observed. However, the lateral load still started to drop at this drift ratio. Thus, the lateral load in the positive loading direction of specimen CH also reached the peak at 4% drift. In contrast, the lateral load was still increasing for specimen CSH in the positive loading direction. It started to drop at 6% drift, later than the other two beams.

The testing of specimens CH, DPH, and CSH was terminated after the second cycle of 6% drift, the second cycle of 5% drift, and the second cycle of 6% drift when the negative load dropped to 27%, 15%, and 25% the peak value, respectively. No fracture of longitudinal and transverse reinforcing bars was observed at the end of the test for specimens CH and DPH, as shown in Fig. 10(a) and (b), respectively. In contrast, for specimen CSH, fractures of longitudinal and transverse reinforcing bars were observed, as shown in Fig. 10(c). This indicates that the stresses of reinforcing bars in specimen CSH were better developed due to better restraint from the intermediate hoops of the CSH than the other two specimens.

Hysteretic behavior

The lateral load and displacement relationships (hysteretic behavior) of specimens CH, DPH, and CSH are shown in Fig. 11(a) to (c), respectively. The envelope responses of

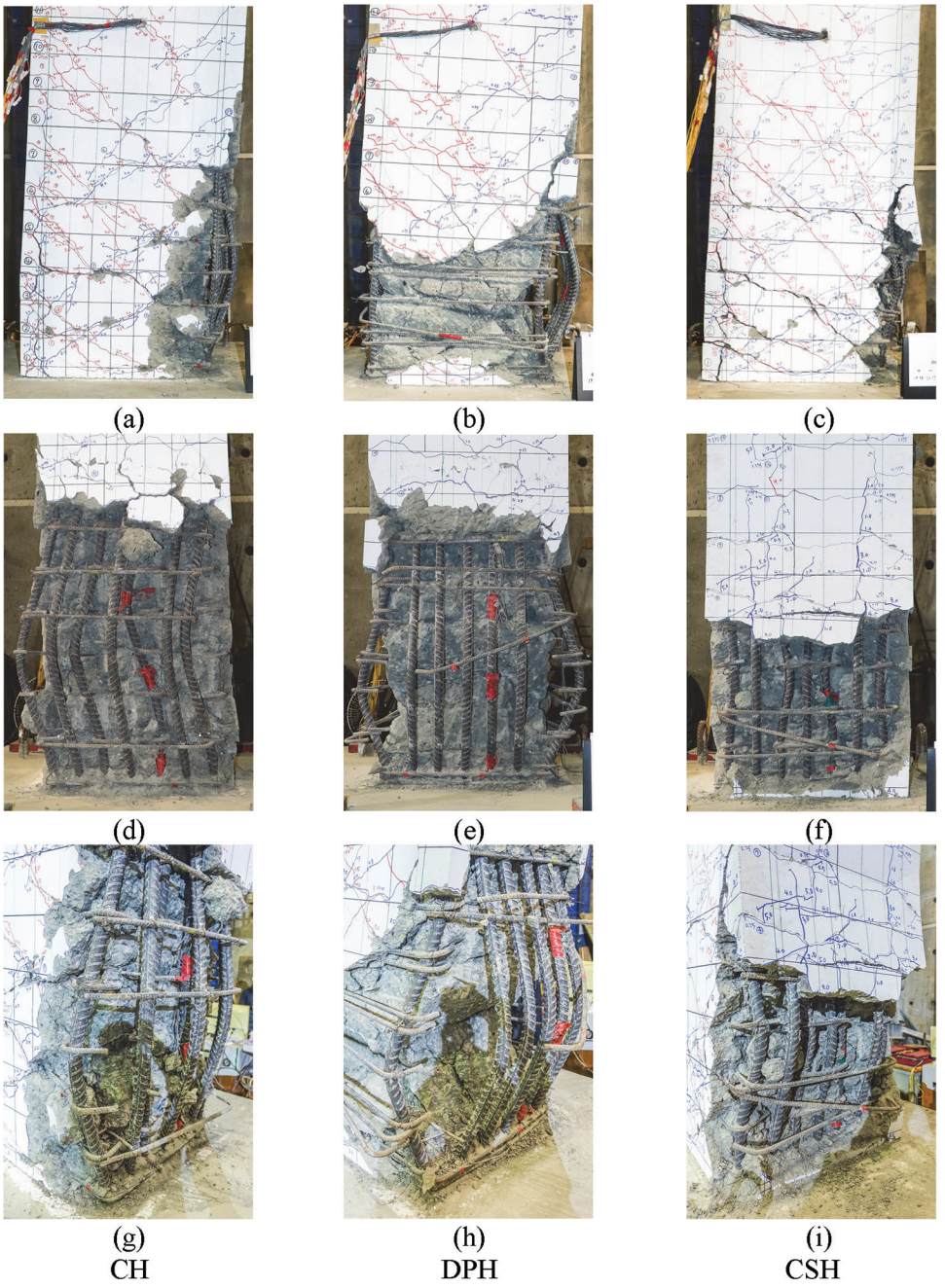

Fig. 9—Damage condition after first cycle of 5% drift on east face (side face) of beam near fixed end for specimens (a) CH, (b) DPH, and (c) CSH; on north face (top face) of beam for specimens (d) CH, (e) DPH, and (f) CSH; and at northeast corner for specimens (g) CH, (h) DPH, and (i) CSH.

all three specimens are compared in Fig. 11(d). To evaluate the ductility (μ) and plastic drift capacity (Δ_p) of the beam, the envelope responses of all three specimens were idealized using the bilinear model from FEMA 356.[19] The bilinear model has two linear segments. The first segment passes through the envelope response at approximately 60% of the yield load ($0.6V_y$) and ends at the yield point. The second segment starts from the yield point and ends at the ultimate drift (Δ_u). The second segment is assumed to have zero stiffness. The Δ_u is defined as the drift when the lateral load drops to 80% of the peak value on the descending branch of the envelope response. The yield point was selected so that the area covered under the bilinear model would be close to the area under the envelope response curve. The μ is defined as the ratio of Δ_u to the drift of the yield point (Δ_y), and the plastic drift (Δ_p) is defined as Δ_u minus Δ_y. The bilinear model parameters and the measured peak lateral load of each specimen are listed in Table 2.

All specimens showed similar hysteretic behavior when the drift did not exceed 4% and 3% in the positive and negative loading directions, respectively. Some pinching was observed for each specimen. The pinching was likely due to shear and/or bond deterioration. Specimen DPH reached the peak load in the positive direction at 4% drift, the same as the control specimen (CH). However, the strength degradation after the peak load of specimen DPH was more severe than

Fig. 10—Close view of reinforcement damage of specimens: (a) CH; (b) DPH; and (c) CSH.

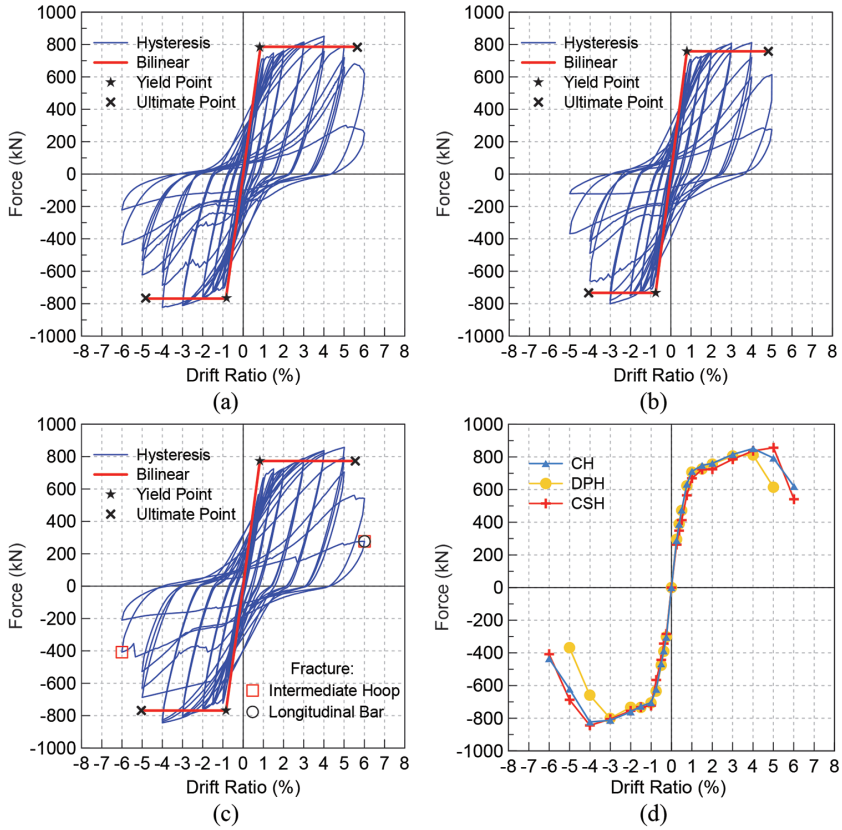

Fig. 11—Hysteretic behavior of specimens: (a) CH; (b) DPH; (c) CSH; and (d) envelope responses of all specimens. (Note: 1 kN = 0.2248 kip.)

that of specimen CH. In the negative direction, specimen DPH reached the peak load at 3% drift, earlier than specimen CH. As a result, the average Δ_u, Δ_p, and μ of specimen DPH were 4.5%, 3.7%, and 5.8, respectively, which were 14%, 16%, and 5% lower than the average Δ_u, Δ_p, and μ of 5.2%, 4.4%, and 6.1 of specimen CH, respectively. As stated previously, the lower drift and ductility capacities of specimen DPH were mainly due to the lack of lateral support to the central five longitudinal bars, leading to earlier and more extensive buckling of the bars in compression. However, specimen DPH still exhibited drift and ductility capacities higher than typically required for beams of special moment frames—for example, 3.5%.[18]

Specimen CSH reached the peak load in the positive loading direction at 5% drift, which is 1% drift later than specimen CH. However, after the peak load, the strength of specimen CSH degraded faster than CH. This was due to the fracture of the longitudinal bars in specimen CSH, resulting from a better restraint by the CSH than the CH. In the negative loading direction, specimen CSH reached the peak load at 4% drift, the same as specimen CH, and showed a slightly lower strength degradation in the beginning than specimen CH but later accelerated due to fracture of the longitudinal bars. The average Δ_u, Δ_p, and μ of specimen CSH were 5.3%, 4.5%, and 6.3, respectively, which were 2%, 2%, and 3% higher than those of specimen CH, respectively. The better

Table 2—Drift capacity and strength ratio

Specimen	Loading direction	Δ_y, %	Δ_u, %	μ	Δ_p, %	V_y, kN	V_{max}, kN	M_{test}, kN·m	M_n, kN·m	M_{test}/M_n	ξ_{eq} 4%, %
CH	(+)	0.86	5.65	6.57	4.79	786	851	2554	1857	1.38	18.80
	(–)	0.85	4.82	5.65	3.97	769	823	2469	1857	1.33	
	Avg.	0.86	5.24	6.11	4.38	777	837	2511	1857	1.35	
DPH	(+)	0.79	4.82	6.09	4.03	758	812	2436	1857	1.31	18.38
	(–)	0.75	4.07	5.42	3.32	734	801	2403	1857	1.29	
	Avg.	0.77	4.45	5.76	3.68	746	806	2419	1857	1.30	
CSH	(+)	0.83	5.55	6.71	4.72	734	857	2570	1857	1.38	20.03
	(–)	0.85	5.04	5.94	4.19	758	844	2533	1857	1.36	
	Avg.	0.84	5.30	6.32	4.46	746	850	2551	1857	1.37	

Note: 1 kN = 0.2248 kip; 1 kN·m = 0.7376 kip·ft.

performance of specimen CSH in drift and ductility capacities was not so significant compared with damage control, as shown in the previous section. However, the beneficial effect of the CSH on the drift and ductility capacities could still be observed.

Also listed in Table 2 is the ratio of the measured average moment strength (M_{test}) to the nominal moment strength (M_n) calculated based on ACI 318-19[1] with actual material strengths. The M_{test}/M_n of specimen DPH was 1.3. Although it is 4% lower than that of specimen CH, it is 30% higher than M_n. This and the observations from the drift and ductility capacities stated earlier showed that despite the lower lateral support to the central five longitudinal bars on the top and bottom sides of the beam of specimen DPH, the specimen still exhibited strength and deformation sufficient for beams of special moment frames. The M_{test}/M_n of specimen CSH was 1.37, which was 1% higher than that of specimen CH. The strength capacity of specimen CSH was similar to specimen CH.

Curvature, bar slip, and shear strain

The curvature, including bar slip and shear strain distributions for each specimen, were calculated based on the space coordinate measurements of the optical sensors attached to the east face of the specimen. Figures 12(a) to (c) show the distributions of the curvature, including the contribution from the bar slip, and Fig. 12(d) to (f) show the distributions of the shear strain. Beam level zero in Fig. 12 represents the fixed end of the beam. Note that the curvature value at beam level zero was mainly due to the contribution from the bar slip. Because the sensors were removed at 4% drift to protect them from being damaged by the severe concrete cracking and spalling occurring at that drift, the curvature and shear strain data were only available up to 3% drift.

It can be seen from Fig. 12 that specimen DPH showed a length with large curvatures of approximately 725 mm (28.54 in.) and a length of large shear strains of approximately 1025 mm (40.35 in.) from the fixed end at 3% drift. These were larger by 26% and 17% than the corresponding lengths observed in specimen CH, approximately 575 and 875 mm (22.64 and 34.45 in.), respectively. This indicated more extensive damage in specimen DPH than CH at 3% drift. However, this more extensive damage at 3% drift did not cause a significant difference in the visual damage and hysteretic behavior, as presented in previous sections.

For specimen CSH, the lengths with large curvatures and shear strains at 3% drift were approximately 575 and 875 mm (22.64 and 34.45 in.), the same as those of specimen CH at the same drift. These observations were consistent with the previous observations on damage and hysteretic behavior in which the two specimens showed similar behavior at 3% drift.

Figure 13 shows the percentage contributions of the curvature, bar slip, and shear strain to the lateral displacement of the beam for each specimen. The lateral displacement due to bar slip was calculated from the curvature value at beam level zero and that due to curvature from the rest of the measured curvatures. For specimens CH, DPH, and CSH at 3% drift, the curvature and bar slip contributed to 85.05, 84.94, and 86.87%, and shear strains contributed to 14.95, 15.06, and 13.13% of the lateral displacement, respectively. All three specimens showed flexural-dominated behavior, with a flexural contribution of more than 85% of the total lateral displacement. The CSH controlled shear deformations better than the other two specimens. The shear strain of specimen CSH at 3% drift was lower by 12% than specimen CH. Specimen DPH showed a very similar level of shear strain at 3% drift to specimen CH.

Energy dissipation

The energy dissipation capacity was assessed using the equivalent damping ratio (ξ_{eq}), as defined in Eq. (1). The ξ_{eq} was calculated for each cycle of the hysteretic response. The average value of the three cycles of each drift level is shown in Fig. 14. Similar values of ξ_{eq} were observed between the three specimens when the drift was equal to or less than 3%. At 4% drift, the ξ_{eq} of specimen DPH started to decrease. The ξ_{eq} was 18.38%, lower by 2% than specimen CH, which was 18.80%. In contrast, the ξ_{eq} of specimen CSH was still increasing. The ξ_{eq} was 20.03%, higher by 7% than specimen CH. At 5% drift, specimen DPH failed, and hence the ξ_{eq} was not shown in the figure. At this drift, the ξ_{eq} of specimen CSH was 18.50%, higher by 39% than specimen CH.

$$\xi_{eq} = \frac{1}{4\pi}\left(\frac{E_D}{E_S}\right) \quad (1)$$

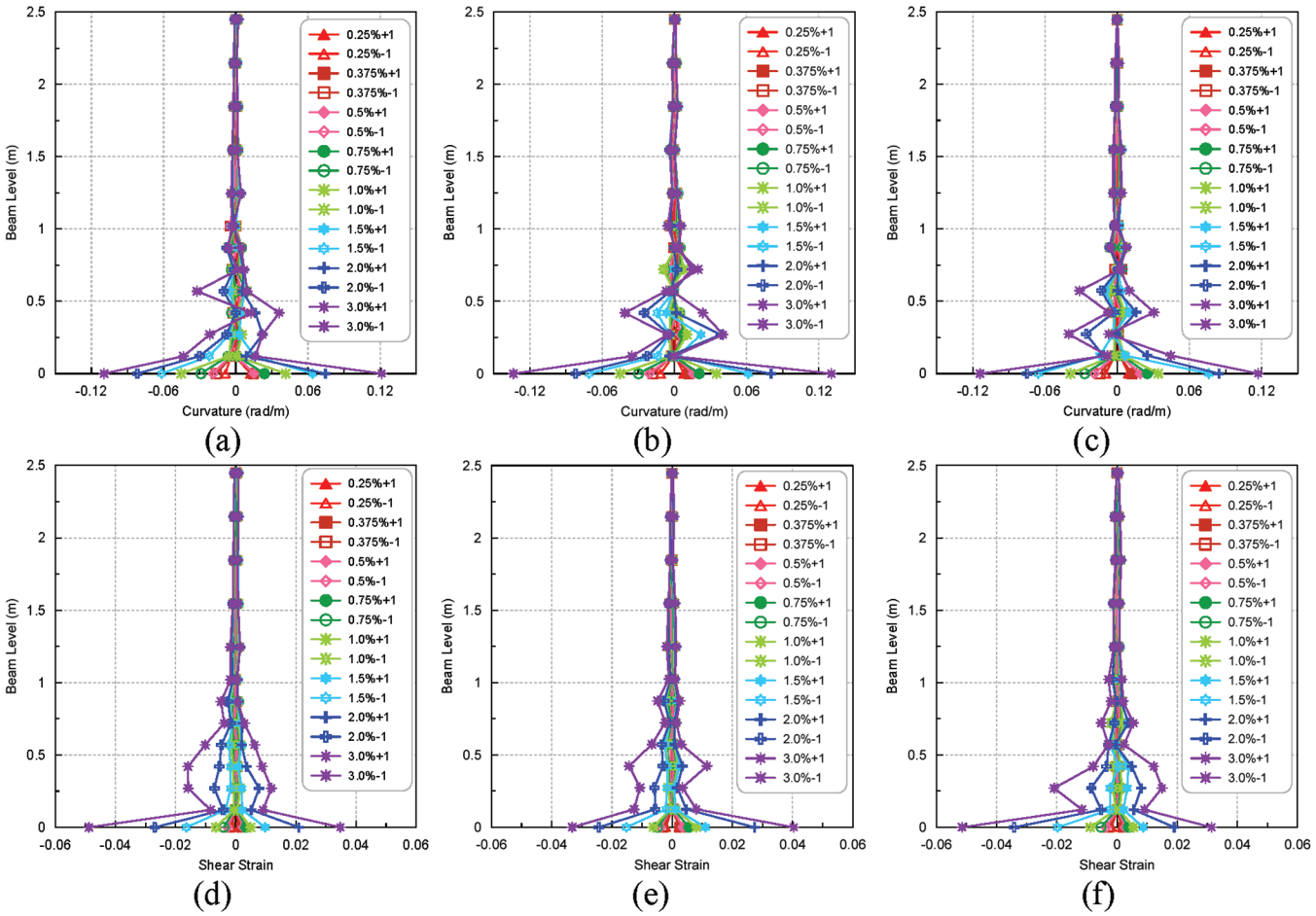

Fig. 12—Curvature distributions of specimens: (a) CH; (b) DPH; and (c) CSH; and shear strain distributions of specimens: (d) CH; (e) DPH; and (f) CSH. (Note: 1 mm = 0.0393 in.)

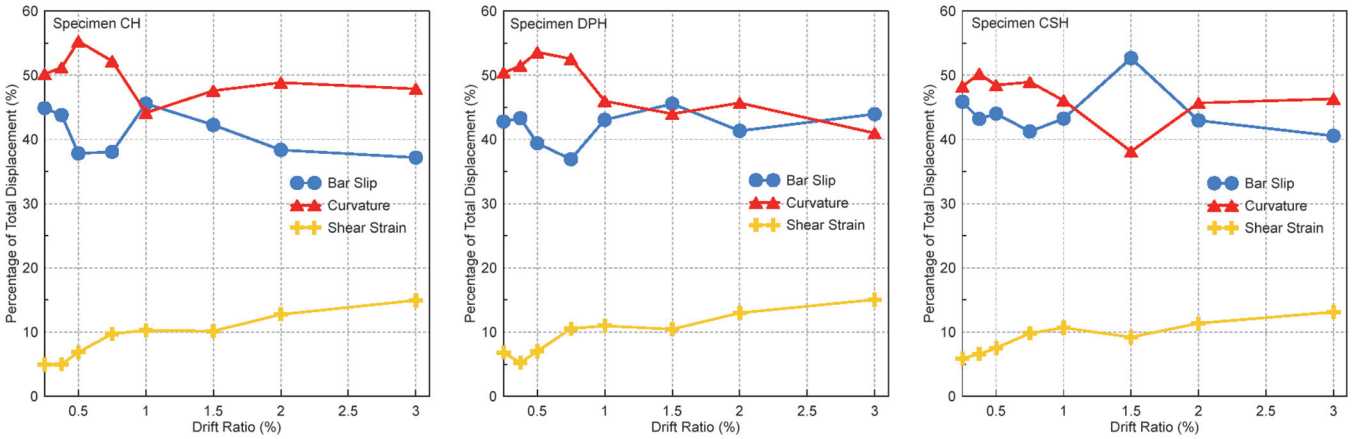

Fig. 13—Percentage contributions of curvature, bar slip, and shear strain to lateral displacement of beam.

From the previous comparison, it can be seen that specimen DPH showed a similar energy dissipation to specimen CH up to 4% drift, which is typically considered sufficient for beams of special moment frames, as stated previously. The lack of lateral support to the central five longitudinal bars on the top and bottom sides of the beam had a significant adverse effect on the energy dissipation only when the drift reached 5%. Specimen CSH showed an energy dissipation capacity superior to specimen CH, starting from 4% drift. This again indicated the better confinement and restraint effect of the CSH than the CH.

Strain gauge analysis

The strain responses of the beam top and bottom longitudinal reinforcing bars from gauges LT, located 350 mm (13.78 in.) from the fixed end of the beams, and gauges LB, located 50 mm (1.97 in.) from the fixed end of the beams, are shown in Fig. 15(a) and (b), respectively. The locations of gauges LT and LB in the beam cross section are shown

in Fig. 5. The responses of specimen CSH at the drifts of 0.375 to 0.5% were lost and hence are not shown. All the specimens showed tensile yielding of longitudinal reinforcing bars at approximately 1% drift, consistent with the yield drift shown in Table 2. No significant differences were observed between the specimens. This is mainly because the strain responses were available only up to 1.5% drift. The damages of the specimens were still minor at this drift ratio.

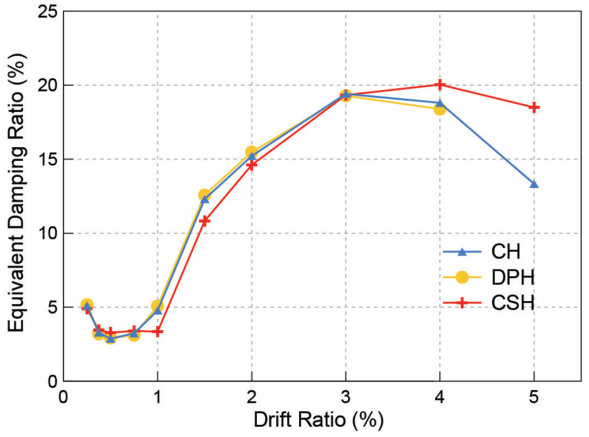

Fig. 14—Equivalent damping ratio.

The strain responses of the perimeter stirrups from gauges TPM, located 350 mm (13.78 in.) from the fixed end of the beams, are shown in Fig. 15(c). The perimeter stirrups of all the specimens developed strains much higher than the yield strain, indicating that the perimeter stirrups with seismic hooks at both ends in these specimens were effectively used to resist cyclic shear and provide restraint to corner longitudinal bars and confinement to concrete. The strain responses of the intermediate stirrups (specimen CH) and intermediate hoops (specimen CSH) from gauges TIM, located 350 mm (13.78 in.) from the fixed end of the beams, are shown in Fig. 15(d). Specimen DPH did not have intermediate stirrups or hoops and hence was not included in the comparison. It can be seen that the strains of the intermediate hoops of specimen CSH were initially similar to those of the intermediate stirrups of specimen CH but were much higher at high drifts. This observation was consistent with the damage observation stated previously, in which the intermediate hoops of specimen CSH showed fracture while the intermediate stirrups of specimen CH did not. This again showed that the intermediate hoops made of a continuous bar could be better mobilized to resist shear, buckling of longitudinal bars, and concrete expansion than the intermediate stirrups with seismic hooks at both ends. The seismic hooks tended

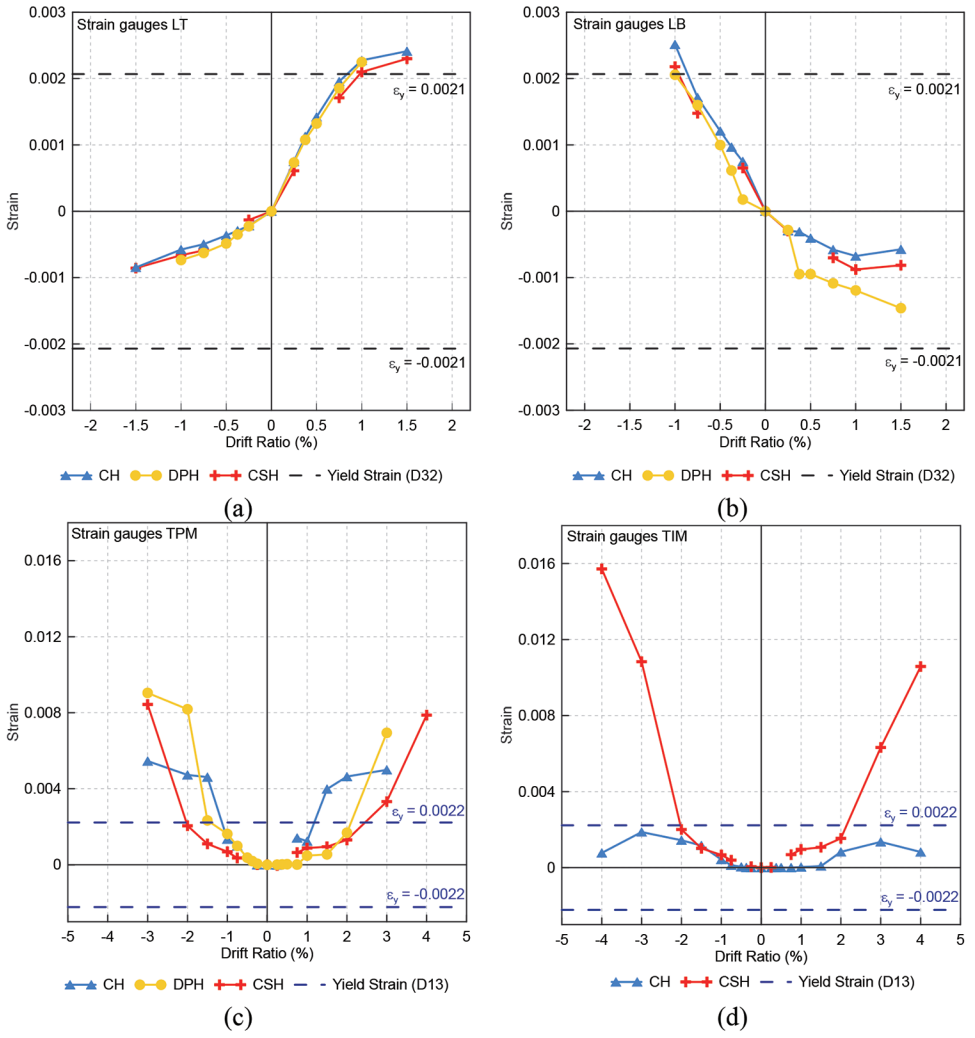

Fig. 15—Envelope responses of strain gauges: (a) LT; (b) LB; (c) TPM; and (d) TIM.

to be pushed out after spalling of cover concrete, as shown in Fig. 9(g). In contrast, the intermediate hoops did not have this problem and hence performed better than the intermediate stirrups.

CONCLUSIONS

Two types of hoop layouts, double-perimeter hoops (DPH) and continuous-stirrup hoops (CSH), with better constructability than conventional hoops (CH), were proposed in this research for the potential plastic hinge region of beams of special moment frames. Three full-scale beam specimens were tested to examine their seismic performance. Specimen CH was designed with conventional hoops and served as a control specimen. Specimens DPH and CSH were designed with double-perimeter hoops and continuous-stirrup hoops, respectively. The DPH used in specimen DPH violated the Code requirements for the number and spacing of laterally supported longitudinal bars in the potential plastic hinge region. Specimens CH and CSH conformed to the Code requirements using intermediate stirrups and hoops, respectively. The following conclusions can be drawn based on the test observations and analysis. Due to budget constraints, only a limited number of specimens were investigated. Care should be taken when extending the interpretation of the test results of this research to beams with different design parameters, such as different longitudinal compression to tension reinforcement ratios, the presence of a slab, and so on.

1. Specimen DPH showed Δ_u, Δ_p, and μ of 4.5%, 3.7%, and 5.8, which were 14%, 16%, and 5% lower than those of specimen CH, respectively. The lower deformation capacities of specimen DPH were mainly due to the fewer laterally supported longitudinal bars. This caused earlier and more extensive buckling of longitudinal bars and more severe concrete damage, particularly near the top side of the beam, where crossties were used. Despite this, the deformation capacities of specimen DPH were still higher than typically required for beams of special moment frames. The M_{test}/M_n and ξ_{eq} at 4% drift of specimen DPH were 1.3 and 18.38%, which were 4% and 2% lower than those of specimen CH, respectively. Furthermore, the DPH showed a similar ability to control the shear deformation of the beam to specimen CH. Despite violating the Code requirements for the number and spacing of laterally supported longitudinal bars, specimen DPH still possessed sufficient strength, deformation, and energy dissipation required for beams of special moment frames. Note that this conclusion is likely only applicable to cases similar to or less critical than specimen DPH, which had 29% of longitudinal bars (two out of seven bars) laterally supported by a seismic hook or the corner of a hoop and the maximum h_x of 562 mm (22.13 in.). A further reduction in the number and increase in the spacing of laterally supported longitudinal bars is expected to decrease the seismic performance.

2. Specimen CSH showed Δ_u, Δ_p, μ, and M_{test}/M_n of 5.3%, 4.5%, 6.3, and 1.37, which were 2%, 2%, 3%, and 1% higher than those of specimen CH, respectively. The ξ_{eq} of specimen CSH were 20.03% and 18.50% at 4% and 5% drift, which were 7% and 39% higher than those of specimen CH, respectively. The shear strain of specimen CSH at 3% drift was 12% lower than that of specimen CH. The better performance of specimen CSH was attributed to the better concrete confinement and reinforcing bar buckling restraint ability of the intermediate hoops (made of a continuous bar) of the CSH than the intermediate stirrups of the CH. The top central three longitudinal bars in CSH were better restrained from buckling than those of CH. The damage severity and extent of specimen CSH were less for a given drift than specimen CH. The proposed CSH can increase the constructability and seismic performance of beams of special moment frames.

AUTHOR BIOS

ACI member **Yu-Chen Ou** *is a Distinguished Professor in the Department of Civil Engineering at National Taiwan University, Taipei, Taiwan. He received his PhD from the State University of New York at Buffalo, Buffalo, NY. He is President of the ACI Taiwan Chapter. His research interests include reinforced concrete structures, earthquake engineering, and bridge engineering.*

ACI member **Hermawan Sutejo** *is a PhD Candidate in the Department of Civil Engineering at National Taiwan University, where he received his master of science in civil engineering. His research interests include earthquake-resistant reinforced concrete structures and finite element modeling of reinforced concrete members.*

Jyun-Lin Huang *is a Civil Engineer. He received his master of science in civil engineering from National Taiwan University.*

Sheng-I Yen *is the Vice President of the Technical Division at Chien Kuo Construction Co., Ltd., in Taipei, Taiwan. He received his PhD from National Yang Ming Chiao Tung University, Hsinchu, Taiwan.*

ACKNOWLEDGMENTS

The authors would like to thank the financial support from Chien Kuo Construction Co., Ltd., and the National Science and Technology Council (NSTC) of Taiwan under Contract No. 109-2221-E-002-003-MY3, and the National Center for Research on Earthquake Engineering (NCREE) of Taiwan for experimental facilities and personnel.

NOTATION

A_g	=	gross area of concrete section
a	=	shear span of beam
d	=	distance from extreme compression fiber to centroid of longitudinal tension reinforcement
d_b	=	nominal diameter of bar and wire
E_D	=	total energy dissipated in isolation system per displacement cycle
E_S	=	effective strain energy
f_c'	=	actual compressive strength of concrete
f_{cs}'	=	specified compressive strength of concrete
f_{ui}	=	ultimate strength of intermediate hoops or stirrups
f_{ul}	=	ultimate strength of longitudinal reinforcement
f_{up}	=	ultimate strength of perimeter hoops
f_{yi}	=	actual yield strength of intermediate hoops or stirrups
f_{yis}	=	specified yield strength of intermediate hoops or stirrups
f_{yl}	=	actual yield strength of longitudinal reinforcement
f_{yls}	=	specified yield strength of longitudinal reinforcement
f_{yp}	=	actual yield strength of perimeter hoops
f_{yps}	=	specified yield strength of perimeter hoops
h_x	=	maximum center-to-center spacing of longitudinal bars laterally supported by corners of crossties or hoop legs around perimeter of column or wall boundary element
M_n	=	beam nominal moment capacity
M_{test}	=	beam maximum moment from testing
P_u	=	factored axial force
V_{max}	=	maximum test lateral force
V_n	=	nominal shear strength
V_u	=	factored shear force at section
V_y	=	lateral force of yield point
Δ_p	=	plastic drift
Δ_u	=	ultimate drift
Δ_y	=	yield drift
ε_y	=	yield strain of reinforcement

ϕ = strength reduction factor, 0.75 for shear
μ = ductility
ρ_l = longitudinal tension reinforcement ratio
ξ_{eq} = equivalent viscous damping ratio

REFERENCES

1. ACI Committee 318, "Building Code Requirements for Structural Concrete (ACI 318-19) and Commentary (ACI 318R-19) (Reapproved 2022)," American Concrete Institute, Farmington Hills, MI, 2019, 624 pp.

2. Mander, J. B.; Priestley, M. J. N.; and Park, R., "Theoretical Stress-Strain Model for Confined Concrete," *Journal of Structural Engineering*, ASCE, V. 114, No. 8, Sept. 1988, pp. 1804-1826. doi: 10.1061/(ASCE)0733-9445(1988)114:8(1804)

3. Pfister, J. F., "Influence of Ties on the Behavior of Reinforced Concrete Columns," *ACI Journal Proceedings*, V. 61, No. 5, May 1964, pp. 521-538.

4. DeGagné, B.; Erdogmus, E.; and Savage, J., "Longitudinal Bar Spacing and Intermediate Ties," *Concrete International*, V. 38, No. 5, May 2016, pp. 43-46.

5. ACI Committee 318, "Building Code Requirements for Reinforced Concrete (ACI 318-63)," American Concrete Institute, Farmington Hills, MI, 1963, 144 pp.

6. ACI Committee 318, "Building Code Requirements for Reinforced Concrete (ACI 318-83)," American Concrete Institute, Farmington Hills, MI, 1983, 111 pp.

7. Elwood, K. J.; Maffei, J.; Riederer, K. A.; and Telleen, K., "Improving Column Confinement: Part 1: Assessment of Design Provisions," *Concrete International*, V. 31, No. 11, Nov. 2009, pp. 32-39.

8. Elwood, K. J.; Maffei, J.; Riederer, K. A.; and Telleen, K., "Improving Column Confinement: Part 2: Proposed New Provisions for the ACI 318 Building Code," *Concrete International*, V. 31, No. 12, Dec. 2009, pp. 41-48.

9. Visnjic, T.; Antonellis, G.; Panagiotou, M.; and Moehle, J. P., "Large Reinforced Concrete Special Moment Frame Beams under Simulated Seismic Loading," *ACI Structural Journal*, V. 113, No. 3, May-June 2016, pp. 469-480.

10. ACI Committee 318, "Building Code Requirements for Structural Concrete (ACI 318-11) and Commentary (ACI 318R-11)," American Concrete Institute, Farmington Hills, MI, 2011, 503 pp.

11. Kang, S.-M.; Park, S.-W.; Jang, S.-W.; Jin, J.-M.; Eom, T.-S.; and Park, H.-G., "Constructability and Economic Evaluation of Continuous Hoop Reinforcement Method," *Journal of the Korea Institute of Building Construction*, V. 13, No. 3, 2013, pp. 291-305.

12. Chalioris, C. E., and Karayannis, C. G., "Experimental Investigation of RC Beams with Rectangular Spiral Reinforcement in Torsion," *Engineering Structures*, V. 56, Nov. 2013, pp. 286-297. doi: 10.1016/j.engstruct.2013.05.003

13. De Corte, W., and Boel, V., "Effectiveness of Spirally Shaped Stirrups in Reinforced Concrete Beams," *Engineering Structures*, V. 52, July 2013, pp. 667-675. doi: 10.1016/j.engstruct.2013.03.032

14. Karayannis, C. G., and Chalioris, C. E., "Shear Tests of Reinforced Concrete Beams with Continuous Rectangular Spiral Reinforcement," *Construction and Building Materials*, V. 46, Sept. 2013, pp. 86-97. doi: 10.1016/j.conbuildmat.2013.04.023

15. Shahrooz, B. M.; Forry, M. L.; Anderson, N. S.; Bill, H. L.; and Doellman, A. M., "Continuous Transverse Reinforcement—Behavior and Design Implications," *ACI Structural Journal*, V. 113, No. 5, Sept.-Oct. 2016, pp. 1085-1094. doi: 10.14359/51689154

16. Bill, H. L.; Miller, M. L.; Doellman, A. M.; and Shahrooz, B. M., "Evaluation of Continuous Transverse Reinforcement," *Concrete International*, V. 35, No. 11, Nov. 2013, pp. 49-55.

17. ASTM A706/A706M-14, "Standard Specification for Deformed and Plain Low-Alloy Steel Bars for Concrete Reinforcement," ASTM International, West Conshohocken, PA, 2014, 7 pp.

18. ACI Committee 374, "Acceptance Criteria for Moment Frames Based on Structural Testing and Commentary (ACI 374.1-05) (Reapproved 2019)," American Concrete Institute, Farmington Hills, MI, 2005, 9 pp.

19. FEMA 356, "Prestandard and Commentary for the Seismic Rehabilitation of Buildings," Federal Emergency Management Agency, Washington, DC, 2000, 518 pp.